Origin of metallicity in atomic Ag wires on Si(557)

2015 New J. Phys. 17 043062

(http://iopscience.iop.org/1367-2630/17/4/043062)

New Journal of Physics
The open access journal at the forefront of physics

Deutsche Physikalische Gesellschaft DPG
IOP Institute of Physics

Published in partnership with: Deutsche Physikalische Gesellschaft and the Institute of Physics

OPEN ACCESS

RECEIVED
27 January 2015

REVISED
21 March 2015

ACCEPTED FOR PUBLICATION
27 March 2015

PUBLISHED
29 April 2015

PAPER

Origin of metallicity in atomic Ag wires on Si(557)

U Krieg, T Lichtenstein, C Brand, C Tegenkamp and H Pfnür

Institut für Festkörperphysik, Leibniz–Universität Hannover, Appelstrasse 2, D-30167 Hannover, Germany

E-mail: pfnuer@fkp.uni-hannover.de

Keywords: plasmons in one dimension, wire doping, high resolution electron loss spectroscopy, tunelling microscopy

Abstract

We investigated the metallicity of Ag-$\sqrt{3}$ ordered atomic wires close to one monolayer (ML) coverage, which are formed on Si(557) via self assembly. For this purpose we combined high resolution electron energy loss spectroscopy with tunneling microscopy. By extending the excess Ag coverage up to 0.6 ML on samples annealed at high temperatures where partial desorption occurs, we demonstrate that one-dimensional metallicity in the Ag-$\sqrt{3} \times \sqrt{3}$ R30° ordered atomic wires on the (111) mini-terraces originates only from Ag atoms in excess of (local) monolayer coverage, which are adsorbed and localized at the highly stepped parts of the Si(557) surface. Thus these Ag atoms act as extrinsic dopants on the atomic scale, causing coverage dependent subband filling and increasing localization as a function of doping concentration. The second layer lattice gas as well as Ag islands on the (111) terraces turn out not to be relevant as dopants. We simulated the peculiar saturation behavior within a modified lattice gas model and give evidence that the preparation dependent saturation of doping is due to changes of average terrace size and step morphology induced by high temperature treatment.

1. Introduction

Plasmons in low-dimensional systems are characterized by a dispersion that starts at zero excitation energy in the long wavelength limit [1, 2] and by group velocities that are typically only of the order of 1% of the speed of light [3, 4]. As a consequence, very short wavelengths of only a few nanometers can be reached, much shorter than those obtained for surface plasmon polaritons, e.g. in graphene [5, 6]. Excitation and energy transfer into these modes, on the other hand, is only possible in the near field of appropriate antennas, if electromagnetic radiation is the source of excitation [7], or by charged particles like electrons, which scatter by an impact scattering mechanism [8]. Because of their short wavelengths, they are interesting candidates for energy transfer and local energy transport on the nanoscale, since extreme localization compared with standard surface plasmon modes should be possible. Linear dispersion, necessary for undistorted signal transfer, can be achieved in these systems by coupling a two-dimensional electron gas (2DEG) with other two- (2D) or three-dimensional electron gases [9], as seen, e.g., for acoustic surface plasmons of Shockley type surface states on surfaces of noble metals, [10–15], or for graphene on metallic surfaces [16, 17].

The dispersion of the one-dimensonal electron gas is already close to linear [18] for an unshielded wire, and therefore particularly attractive. Investigations of metallic arrays of quasi-1D wires, exhibiting quasi-linear 1D dispersion, are still scarce. Examples are studies of metallic and of silicide chains on flat and stepped Si substrates [4, 19–22] with intrinsic metallicity.

A different situation arises when the system is semiconducting or semi-metallic. Here doping with atoms acting as charge acceptors or donors is the method generally used to enhance conductivity in such a material. Indeed low energy 2D plasmons have been found in degenerately doped metal-oxide-semiconductor field-effect transistors and in GaAlAs quantum well structures [23, 24]. In the study presented here, we show that this concept can be extended down to the atomic scale even for quasi-1D systems. Only the doping mechanism becomes more exotic. Doping now happens laterally and, for the example studied here, even by atoms of the same kind, which are bound differently to the substrate than the majority. We call this mechanism extrinsic self-doping.

The doping mechanism of the coverage dependent insulator-metal transition in the quasi-1D system observed for silver adsorbed on Si(111) and on the regularly stepped Si(557) surface close to monolayer coverage has been under debate for several years [25–28]. As it turns out, similar to Ag monolayers on flat Si(111) [29], an Ag-$\sqrt{3} \times \sqrt{3}$ R30° structure of monolayer coverage is formed on the (111)-oriented mini- terraces for Ag/Si (557), and metallicity seems to be coupled to the formation of the $\sqrt{3}$ - structure on the (111)-oriented minifacets [27]. These Ag wires of single atomic height are separated by (112)-minifacets with three double-steps, which act as non-conducting separators, so that 1D metallicity was observed [27]. Similar to Ag/Si(111) [30], these wires are semi-metallic for the perfect Ag-$\sqrt{3}$ structure, but become metallic when extremely small amounts of Ag are added [28], which act as self-dopants. Doping may be caused by a lattice gas in the second layer on the (111)-terraces or by inhomogeneities on a surface such as defects, step edges etc. They may provide binding sites with electronic properties significantly different from the flat terrace, so that the atoms bound there become partially ionized. Here we present a detailed study of this question, yielding a unique answer in favour of the second mechanism.

First we briefly summarize the present knowledge on the Ag/Si(557) system [27, 28]. If the Ag monolayers are prepared at 500 to 520 °C, they contain a saturation density of charge carriers, but these charge carriers, obviously coupled with some excess coverage of Ag, can be removed by partial desorption of Ag at temperatures around 600 °C, leaving average coverages between 0.8 and 0.9 ML on the surface. As low energy electron diffraction (LEED) profile analysis shows, the Ag-$\sqrt{3}$ structure only loses up to 20% of its intensity, but the spot profiles remain as sharp as after preparation. In other words, the Ag layers now exist as very long $\sqrt{3}$ -ordered strips, i.e. the length of the $\sqrt{3}$ -ordered Ag strips is still of the order of 1 μm, which do not cover the whole surface anymore. These layers don't exhibit any plasmonic losses, as investigated in our experiments using high resolution electron energy loss spectroscopy with both high energy and momentum resolution (ELS-LEED). However, post-adsorption of tiny amounts of Ag on these layers (0.002–0.05 ML) restores metallicity even at the smallest controllable Ag concentrations.

While these properties just described already rule out the existence of a lattice gas in the second Ag layer as long as the first monolayer is incomplete, and thus the lattice gas as the source of metallicity, the aim of the present paper is to yield further insight into the doping mechanism, which is fully compatible with 'extrinsic' doping by partial charge transfer from Ag atoms adsorbed on the (112)-facets outside the (111)-oriented terraces, i.e. at the triple steps of the Si(557) surface. Carrying out tunneling microscopy experiments on surfaces prepared by different annealing steps, we find that the sensitivity of saturation concentration of charge carriers on preparation conditions is related to changes of step morphology, which is fully in agreement with the model of extrinsic doping of the Ag quantum wires. For a more quantitative description of this scenario, we develop an adsorption model that describes the experimentally found dependence of loss energy on excess Ag coverage. As we also show, this model of extrinsic doping is capable of qualitatively explaining also the observed effect of increasingly stronger localization as we increase the doping concentration. Reliable and precise calibration of the Ag amount adsorbed to the level below one percent was necessary for these experiments, which is described in detail in the Appendix. Furthermore, we will explain in detail our procedure of data evaluation, since our EELS-measurements have to be carried out over long times so that they are susceptible to effects by residual gas adsorption, especially at the smallest excess concentrations of Ag.

2. Experimental details

The plasmons were measured by using a combination of high resolution electron loss spectrometer (EELS) as electron source and detector, combined with the electrostatic deflector of a LEED instrument, thus providing simultaneously high energy and high momentum ($k_{||}$) resolution [31, 32]. Typical operating parameters were 25 meV energy resolution and a $k_{||}$ resolution of 1.3×10^{-2} Å^{-1}. In order to check the surface after *in situ* cleaning and after Ag adsorption, SPA-LEED pictures were taken (SPA means spot profile analysis). Ag was evaporated from a molybdenum crucible by electron-beam heating and the amount was controlled by a quartz microbalance. In order to accurately control the Ag flux, this microbalance was calibrated by a second one placed at sample position. This calibration was verified by calculations and tests with tunneling microscopy in a separate chamber. From these tests we estimate our maximum uncertainty of absolute coverages to be about 5%. The coverage is given with respect to the Si(111) surface density, i.e. 1 ML corresponds to 7.83×10^{14} atoms per cm^2. Samples were prepared by repeated flash annealing to 1100 °C with a quench to 900 °C and linear cooling to 800 °C over 2 min. 1.2 ML Ag was evaporated on the sample held at 500 °C. This amount was chosen to compensate for the silver loss during the partial desorption steps in order to remove the dopant and to still remain close to 1 ML average coverage at the end of this procedure. In order to prepare an undoped semiconducting Ag-$\sqrt{3}$ surface, we used the annealing procedure already described and characterized in [28].

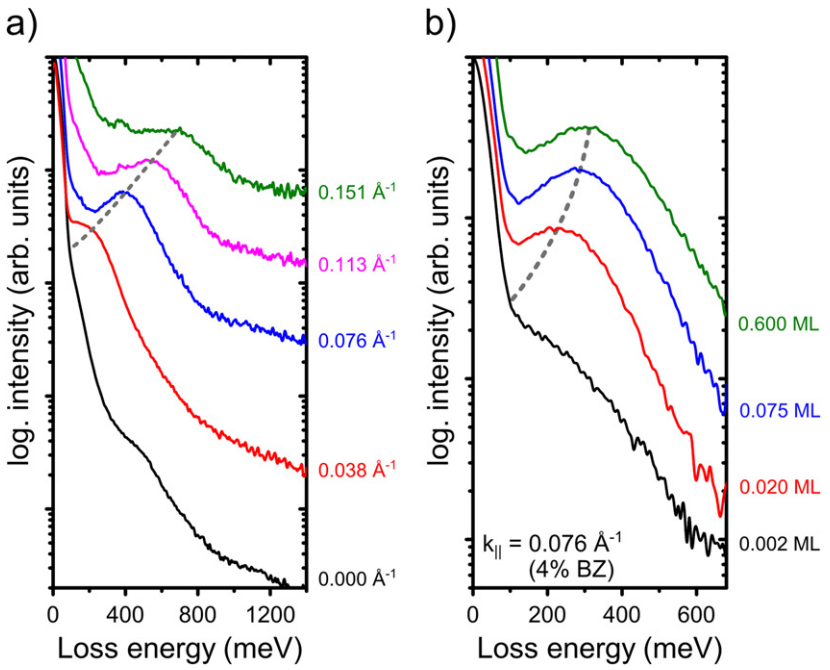

Figure 1. (a) Electron energy loss sample spectra at a constant excess coverage of 0.2 ML measured in the direction along the wires as a function of $k_{\|}$ for the values given as parameters. The elastic peak is at loss energy zero. (b) Same for constant $k_{\|} = 0.076$ Å^{-1} (4% BZ) as a function of excess concentration. Spectra (log scale for intensity axis) were shifted for clarity. Primary energy: 20 eV.

3. Results and discussion

3.1. Doping via adsorption of silver adatoms

Sets of typical loss spectra observed at constant Ag excess coverage with a doping concentration close to maximum are plotted in figure 1(a) as a function of parallel momentum. They show the low-energy 1D plasmon losses. Their dispersion scales almost linearly with $k_{\|}$, as expected for a 1D system [27]. Using the measurement procedures described in appendix A, we were able to completely exclude effects from the residual gas. The results obtained here extend those obtained and described in [28]. The analysis of the spectra shown in figure 1(a), in particular the precise determination of the peak positions of plasmonic losses, is described in appendix B.

Sample spectra as a function of Ag excess concentration, but at constant $k_{\|}$ are shown in figure 1(b). For these spectra we have recently shown [28] that their peak positions scale with the Ag excess coverage as $E_{\mathrm{loss}} \propto \sqrt{n_e}$ at low Ag coverage, where we can safely assume that the concentration of free charge carriers, n_e, is proportional to $\delta\Theta$, the Ag excess concentration. The peak positions of the loss spectra as a function of $\delta\Theta$ are shown in figure 2 as a function of excess Ag coverage. Please note that these data have been normalized to the saturation value obtained for Ag monolayers adsorbed at 500 °C taken from [27] for the various $k_{\|}$ values. The dispersion along the wires is thus eliminated by this normalization, and all data should fall on a common line.

While the data in the low doping regime (<0.030 ML) agree well with those previously published, our new data show that there is an abrupt change in doping efficiency as a function of Ag excess concentration close to 0.035 ML. At higher concentrations the loss energy still increases slowly with increasing Ag concentration, but even at 0.6 ML of excess coverage, where large Ag islands of the second layer must already be formed, the loss energy has only risen by an additional 30%. Intriguingly, saturation around 0.7 is obvious after doping close to room temperature, significantly lower that the saturation concentration reached after direct adsorption of the whole layer at 500 °C.

These findings at first glance still seem to be compatible with the formation of a lattice gas in the second Ag layer on the (111) oriented terraces, as proposed by several authors for the flat Ag/Si(111) system [25, 26, 33]. Indeed, experiments have shown that silver in excess of 1 ML forms a 2DEG on the 2D Ag-$\sqrt{3}$ surface [30, 34, 35], which was observable at low temperature. The critical coverage at room temperature was estimated to be 0.03 ML [33], not far from the value obtained in our measurements. Indeed, silver atoms in the second layer at room temperature are highly mobile and are thermally transported to the step edges, where they will be reflected or nucleate [36].

However, although the conducting part of the Ag/Si(557) system are the (111)-oriented terraces, a lattice gas as electron donor has properties that are in obvious conflict with our findings for this system:

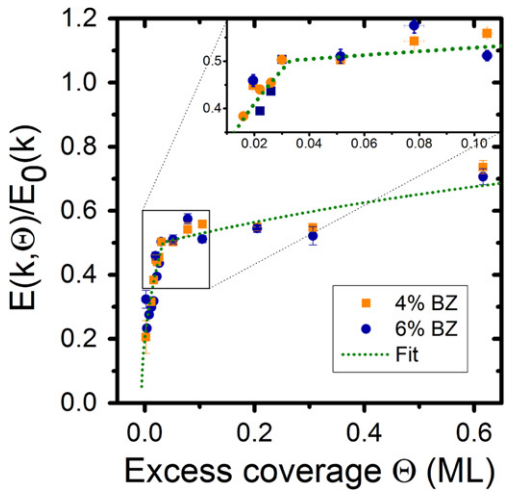

Figure 2. Loss energy versus the excess coverage of silver normalized by the loss energy at maximum doping for each individual value of $k_{\|}$ (saturation values taken from [27]). The normalization eliminates dispersion effects so that all data points should fall on a common line. The plasmon was measured at 4% BZ (squares) and 6% BZ (circles, 1% BZ corresponds to $k_{\|} = 0.0189$ Å^{-1}) parallel to the steps with a primary energy of 20 eV. Thick dotted line: fit with the model described in section 3.3. Inset: enlargement of the data section marked by black square.

(a) The saturation density of a lattice gas is an equilibrium property and is strongly dependent on temperature. Therefore, also our critical concentration, where the abrupt change of slope occurs, should depend on temperature. We checked carefully, but were not able to find any temperature dependence of the loss spectra in the range from 100 to 400 K.

(b) Our preparation of the layers, described in detail in [28], shows that we can observe the loss features described here at an average Ag coverage significantly below one monolayer. For these low Ag concentrations a lattice gas in the second layer would not be stable for simple thermodynamic reasons.

(c) Starting our experiments with less than monolayer coverage, we never find any indication that we first have to fill up the first monolayer before entering the metallic state. Instead, doping starts right away with the tiniest amount of Ag added to a layer prepared by high temperature partial desorption.

(d) Doping saturation depends on the preparation method of the layers, which, as we show below, changes the step structure on the surface. The saturation concentration of a lattice gas on the (111) terraces, however, should not be changed by step structures.

(e) Last but not least, residual gas can also act as dopant, which clearly does not require formation of a lattice gas.

This leads us to the suggestion that doping is extrinsic with respect to the Ag-covered (111)-terraces, i.e. the Ag atoms responsible for doping are located at the steps. As suggested by the partial desorption experiments, these atoms are less strongly bound to the Si surface than those on the (111) terraces resulting in electron donation to the Ag-$\sqrt{3}$ terraces. A schematic of this model is shown in figure 3. Here we assume that Ag atoms landing in the second layer on the flat terraces during adsorption are not stable there, but diffuse to the facetted areas, where they become trapped. These areas are marked in red in the lower part of figure 3. Details will be described in section 3.3.

3.2. Step morphology

The question why the saturation doping level depends on the preparation method can be clarified comparing the step morphology as obtained after preparation of a monolayer of Ag at 500 °C with that after partial desorption of Ag at 600 °C, leaving a coverage of about 0.9 ML on the (111)-terraces, as shown in figure 4.

As already shown earlier [27], the preparation of a monolayer of Ag on Si(557) at 500 °C not only forms a monolayer of Ag-$\sqrt{3}$ on the (111) mini-terraces. These terraces are slightly larger than on the clean Si(557) surface — the average terrace width increases from 2.9 to 3.6 nm, and the three steps within the (557) unit cell are shifted closer together so that the original (112)-facet turns into a (113)-orientation. Furthermore, the step edges form characteristic triangles, most likely because complete unit cells of the Ag-$\sqrt{3} \times \sqrt{3}$ R30° structure are most stable, a condition that cannot be fulfilled with straight steps in $[1\bar{1}0]$ direction.

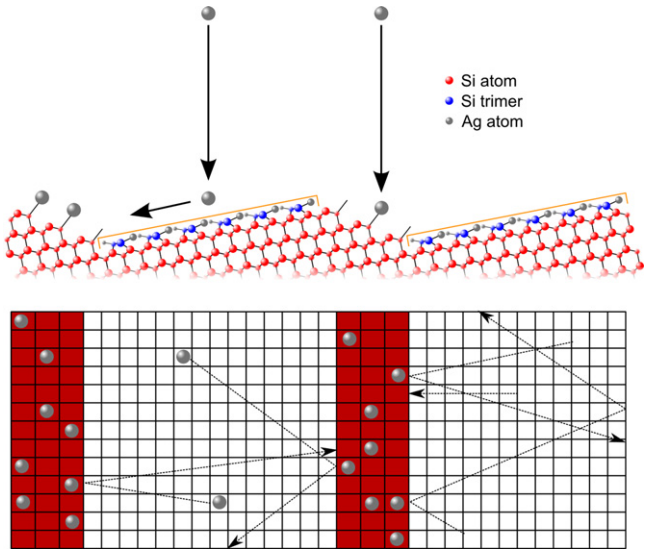

Figure 3. Schematic (side and top views) illustrating the edge doping mechanism. The Si(557) surface with the Ag-$\sqrt{3}$ wires on the (111)-oriented terraces is shown. The area with doping adsorption sites is marked in red, whereas for adsorption the whole surface except already occupied sites is available.

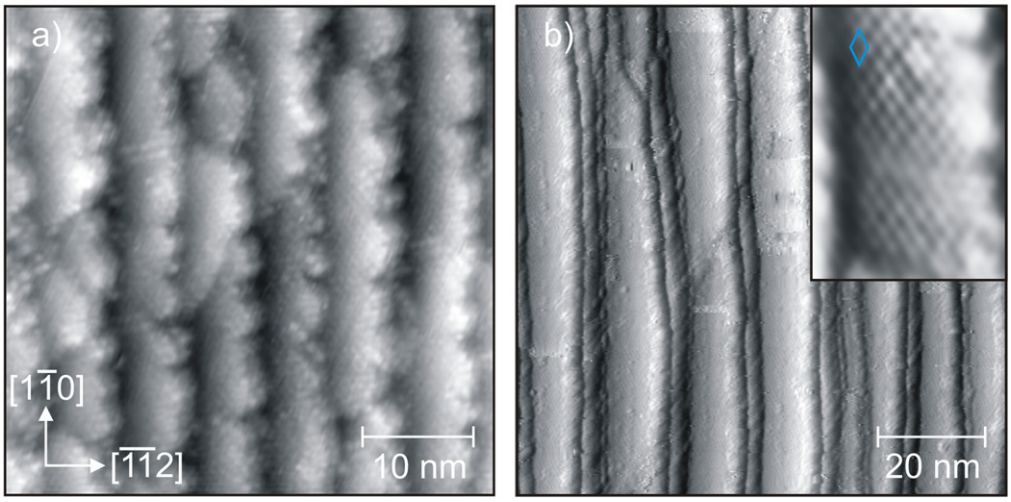

Figure 4. Step morphology of Ag/Si(557) monolayers by STM images taken at 40 K. (a) After preparation of 1.2 ML at 500 °C. (b) After partial desorption at 600 °C, mainly from the stepped part of the surface, with a remaining Ag-$\sqrt{3}$ coverage of 0.9 ML. Clearly visible is that the average step width has roughly doubled. Inset (7.4 × 10.4 nm^2): surviving Ag-$\sqrt{3}$ × $\sqrt{3}$ R30° structure on (111) terraces. Image (a) recorded at 2 V, 150 pA, (b) 1 V, 150 pA, inset at 260 pA.

Unexpectedly, partial desorption at 600 °C not only leads to preferential desorption from the steps, as concluded in our previous publication [28]. As now revealed by detailed STM investigations and demonstrated in figure 4(b), the (557)-surface turns out to be unstable under these conditions. It tends to form larger (111)-oriented terraces, which are now between 7 and 10 nm wide, separated by correspondingly larger step arrays in order to maintain the macroscopic inclination. Furthermore, compared to the situation at 1.2 ML, the steps transform from the triangular shape back into straight sections with kinks.

This transformation of terrace and step morphologies has important consequences on the saturation electron densities achievable by edge doping, and directly explains the discrepancy between saturation densities obtained by the two different preparations just mentioned. Directly related with the increasing average size of (111) terraces, the concentration of edge sites adjacent to these terraces is reduced, as is the maximum Ag concentration per edge chain and unit length due to the straightening of the steps. If exclusively the adjacent edge sites were effective for doping, we should observe a reduction to less than half of the effective saturation

concentration comparing our present results with those of the Ag layer prepared in one step at 500 °C. This directly demonstrates that there are also contributions from Ag covered steps further away from the terraces.

This dependence on terrace widths and step morphology once again, and now most directly, rules out the possibility that a lattice gas is responsible for doping here. Within the latter model no dependence on terrace size is expected for the saturation concentration of doping.

3.3. Fit model

Based on this knowledge, we will now simulate the adsorption kinetics and the change of plasmon frequency as a function of Ag excess coverage by using a lattice gas model in order to understand more quantitatively our experimental findings shown in figure 2. We only simulate the situation where the step sites are initially uncovered and the (111) terraces are covered by a full monolayer of Ag. Since there are competing models in the literature even for the clean Si(557)-(7 × 7) reconstructed surface [37, 38] we cannot dwell on the exact adsorption sites of the silver dopants. What we do know though is that the surface can be roughly divided into two regions: The stepped parts and the terraces with the Ag-$\sqrt{3}$ nanowires. For the steps, we discriminate only between those step edges adjacent to the (111)-oriented mini-terraces and all others, since we assume that silver atoms diffusing on the nanowires are chemisorbed at the adjacent step edges, where they are effectively collected before they can reach other steps. An alternative adsorption path is direct adsorption. This means that the collecting effect of the nanowire is switched off once the periphery of the step edges is completely decorated with silver atoms. We further assume that an incoming silver atom that hits an already occupied adsorption site (in the first layer at the step edges, in the second layer on terraces) is reflected back into vacuum, but that otherwise the trapping probability, s, for trapping at the surface during the first encounter is the same everywhere and constant. Since we are considering only the low coverage range, this assumption is of minor importance, but it reduces the number of parameters significantly.

Within this model the adsorption probability is given by:

$$P\left(\Theta_m, \Theta_e\right) = \underbrace{\frac{s}{N_s}\left(N_m - \Theta_m\right)}_{=P\left(\Theta_m\right)} + \underbrace{\frac{s}{N_s}\left(N_e + N_t - \Theta_e\right)H\left(N_e - \Theta_e\right)}_{=P\left(\Theta_e\right)}. \tag{1}$$

With $\Theta = \Theta_e + \Theta_m$ we denote the density of dopants already adsorbed on the surface, Θ_m at the middle and Θ_e at the steps adjacent to the terraces, whereas N_m, N_e, N_t and N_s mark the density of all adsorption sites available at the middle steps, the adjacent steps, on the nanowires, and the total density ($N_s = N_m + N_e + N_t$), respectively. H is the Heaviside step function. In this equation the first term describes direct adsorption at the middle step, whereas the second term at adjacent steps contains both direct adsorption and the effective collection of all Ag atoms landed on wire sites N_t, i.e. an infinite number of attempts is allowed to find an appropriate site at an adjacent step, without taking into account migration to the middle step. This process stops when Θ_e reaches N_e.

The concentration of adsorbed dopants is calculated by integrating over the amount of silver offered to the surface (M) times the adsorption probability $P(\Theta_m, \Theta_e)$, solved with the boundary condition that for $M = 0 \Rightarrow \Theta = 0$:

$$\Theta_m(M) = \left(1 - \exp\left(-\frac{s}{N_s}M\right)\right)N_m, \tag{2}$$

$$\Theta_e(M) = \begin{cases} \Theta_e < N_e & : \left(1 - \exp\left(-\frac{s}{N_s}M\right)\right)\left(N_e + N_t\right) \\ \Theta_e \geqslant N_e & : N_e \end{cases}. \tag{3}$$

If we start at a non-zero level of doping, the corresponding offset can be incorporated via the transformation $M \rightarrow M - M_0$.

The transformation of Θ into an energy loss works as follows: from the measured dispersion of $E(k_\parallel, n_e)$ as a function of $k_\parallel$ [27] and as a function of the electron density n_e ($E \propto \sqrt{n_e}$) [28] we can write:

$$E\left(\Theta, k_\parallel\right) \propto E\left(k_\parallel\right)\sqrt{\Theta(M)}. \tag{4}$$

We assumed that every silver atom donates the same amount of electrons into the surface and that the momentum dependence can be separated from the dependence on charge carrier density. Forming the relative energy loss the proportionality constant disappears:

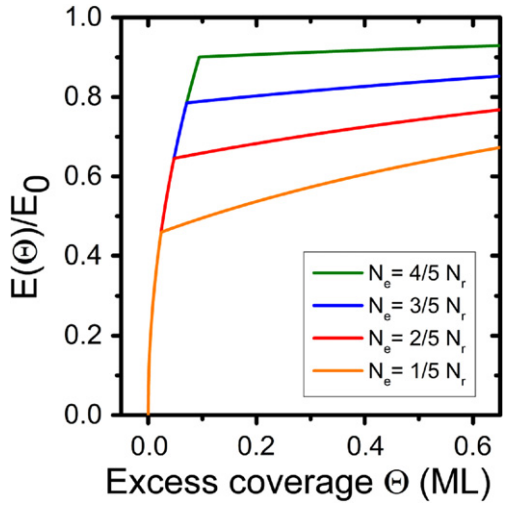

Figure 5. Simulated dependence of the normalized loss peak positions on Ag excess concentration, using the model of step doping (see text) for various critical concentrations N_e.

$$\frac{E\left(\Theta, k_{\|}\right)}{E\left(\Theta \to \infty, k_{\|}\right)} = \frac{E(\Theta)}{E_0} = \frac{\sqrt{\Theta(M)}}{\sqrt{N_r}}, \tag{5}$$

$$= \begin{cases} \Theta_e < N_e & : \frac{1}{\sqrt{N_r}} \sqrt{\left(1 - \exp\left(-\frac{s}{N_s} M\right)\right) N_s} \\ \Theta_e \geqslant N_e & : \frac{1}{\sqrt{N_r}} \sqrt{\left(1 - \exp\left(-\frac{s}{N_s} M\right)\right) N_m + N_e} \end{cases}. \tag{6}$$

Here we introduced $N_r = N_m + N_e$. With this model we can quantitatively describe the observed behavior of the concentration dependence of the plamonic loss peaks shown in figure 2. In order to understand the general systematics, we simulated the doping dependence on Ag excess coverage using various ratios N_e/N_r. The result is shown in figure 5. As can be seen from this figure in comparison with figure 2, the step rise, which ends at $E(\Theta)/E_0 = 0.52$ in figure 2, corresponds to a ratio of $N_e/N_r \approx 0.27$ and to a total excess coverage of 0.035 ML. Assuming on average 20 atomic rows per (111) terrace and the collection of all excess Ag at the two adjacent step edges into single atomic chains, a concentration of 1/3 of the substrate density or 1 excess Ag atom per Ag-$\sqrt{3}$ unit cell and per terrace results. This concentration with barrier-free incorporation into the step edge corresponds to one dopant Ag atom per Ag-$\sqrt{3}$ unit cell along each step edge. Complete saturation is then reached when the equivalent of three such chains is formed.

Interestingly, all other Ag atoms in excess of one monolayer do apparently not contribute to the electron density of this quasi-1D electron gas generating the low energy 1D plasmon. In particular, this seems to be valid for a lattice gas that may still be formed on the terraces, and for 2D islands formed in the second layer on the (111) terraces or in the first layer on the stepped part of the surface. While those on the stepped parts of the surface may still be semiconducting, the islands on the (111)-oriented mini-terraces are definitely metallic. A possible explanation for their invisibility in the range of loss energies studied here may be their small size coupled with a wide size distribution. The small size shifts the lowest excitation to higher loss energies due to confinement effects, while the wide size distribution smears the characteristic plasmon losses over a wide energy window. Generally these low-energy plasmon modes have a low excitation cross section so that they may not have been detected. However, no systematic investigations have been carried out yet concerning this question.

3.4. Extrinsic doping: plasmon localization

The fact that the effective wire width depends on the conditions of preparation has interesting consequences also for the quantum well states seen in the direction **normal** to the wires. Instead of quantum well losses at 470 and 1170 meV in the 1.2 ML layer [28] prepared at 500 °C, here we find losses around 120 and 310 meV at saturation doping concentration. From these findings it seems that we just have scaled down the former loss energies by roughly a factor of four, which is to be expected in a rectangular 1D quantum well when the size is increased by a factor of two. These losses, however, do not appear simultaneously in our new experiment. While the 120 meV

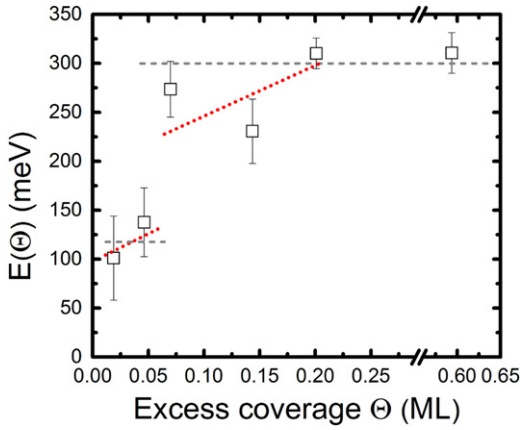

Figure 6. Energetic positions of losses due to quantum well excitations measured at $k_{\|} = 0$ and at various angles normal to the wires. Only averaged data are shown. Lines are guides to the eye for various models (see text).

loss is dominant at Ag excess concentrations below 0.05 ML, the loss above 250 meV (saturating at 310 meV) is mainly seen at higher excess coverages. Therefore, this sequence may be explained better by gradual filling of subbands and dominant transitions from subband 1 to 2 below 3.5% ML and, after starting to fill also subbband 2, from subband 2–3 at higher excess concentrations. Only the second peak can be observed in the fully saturated layer, which would correspond to a reduction factor of only 1.5 in the present case. A possible reason are further localization effects not yet considered (see below), but present also in the broad wires. This assignment, on the other hand, would roughly be compatible with a very shallow further loss around 700 meV in the broad wires, clearly visible only close to saturation. This peak would then correspond to the 1170 meV loss in the narrow wires and to the transition between subbands $2 \rightarrow 4$.

These findings are in fact compatible with our extrinsic doping model. As demonstrated by our experiments, Ag atoms in the monolayer on (111) terraces must be more strongly bound than those on the step edges of the (113) facets. This follows from partial thermal desorption, which preferentially desorbs Ag atoms at steps and erases metallicity of the remaining Ag nanowires, and from the possibility to restore metallicity by adsorption of arbitrarily small amounts of Ag on the semi-metallic wires. This doping mechanism can be rationalized assuming that the Ag-5 s level at the step edges after chemisorption is located above the Fermi level of the Ag monolayer on the (111) terraces, resulting in partial ionization of the Ag 5 s level at step edges and in electron donation to the Ag modified S1 surface band of the Ag wires after equilibration, as indicated schematically in figure 7.

There are several interesting consequences of this scenario. Firstly, it explains the nearly constant charge donation per Ag atom over the limited range of concentrations up to about 3.5% of a monolayer. Adatoms located in chains not adjacent to the wires, which according to our adsorption model are only accessible by surmounting a diffusion barrier, may in addition also be less effective as charge donors. Secondly, the effective dipole per unit length formed at the step edges results not only in charge donation to the wires, but also in band bending at the wire edges. The size of this band bending must also depend on concentration. As a consequence, the spatial electron distribution in the S1 band is modulated by band bending, and we expect increased localization as a function of excess Ag concentration.

The latter effect is actually seen in our studies of quantum well transitions normal to the wires (at $k_{\|} = 0$) as a function of Ag excess coverage shown in figure 6, which turn out to be coverage dependent. Both excitations around 120 ± 30 meV and the prominent loss at 270 meV, respectively, have a clear tendency to increase with Ag concentration. This trend can be explained by increased localization and uneven distribution of electron density within the quantum well due to gradual build-up of edge dipoles, as visualized by figure 7. Indeed, the optimal fit of the dispersion for the narrow wires generated at 500 °C was obtained for a wire widths of 2.4 nm compared with the geometrical width of 3.6 nm [39], which further supports this argumentation.

4. Summary

The system Ag-$\sqrt{3} \times \sqrt{3}$ R30° on the stepped Si(557) provides the unique possibility to unravel the mechanism of charge transfer into atomic wires of the Ag monolayer, which turns out to be semi-metallic. Self-doping by adding an excess concentration of Ag to the local Ag-$\sqrt{3}$ monolayer was observed thus creating an array of quasi 1D metallic wires.

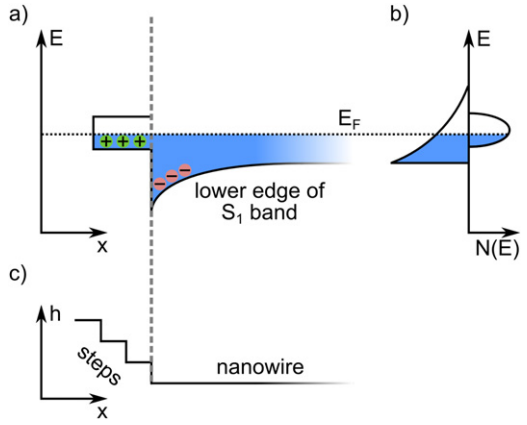

Figure 7. (a) Schematic of partial electron donation to Ag wires on (111) terrraces by Ag atoms adsorbed at step edges. As a consequence, chains of dipoles are formed along the boundaries of the wires, resulting in band bending which depends on concentration (and size) of the dipoles. (b) Scheme of the density of states (DOS) formed by this process. Please note the bottom of this quasi-1D DOS is smeared due to the inhomogeneity at the wire edges. (c) Sketch of the real space configuration.

The doping mechanism by self-doping due to adsorption of Ag atoms at the edges of the (111)-oriented terraces with monolayer coverage was most directly proven by discovering the variability of average terrace sizes caused by high temperature annealing in presence of the Ag monolayer. This caused the saturation concentration of doping to change correspondingly. This mechanism was further corroborated by modelling the adsorption process of excess Ag coverage, assuming both direct adsorption and collection of all Ag atoms initially adsorbed in the second Ag layer at the step edges of the (113) facets. Thus we can safely exclude a doping mechanism by a lattice gas adsorbed in the second Ag layer.

This extrinsic doping mechanism on the nanoscale has important consequences on the uniformity of the confinement potential, and leads to concentration dependent further localization of the electron gas within the wires.

Acknowledgments

Financial support by the Niedersächsisches Ministerium für Wissenschaftund Kultur through the graduate school 'contacts in nanosystems' and by the Deutsche Forschungsgemeinschaft through FOR1700 (project E4) is gratefully acknowledged. We also thank T Inaoka for carrying out further simulations related to this study. We also acknowledge support by the Open Access Publishing Fund of Leibniz Universität Hannover.

Appendix A. Determination and compensation for residual gas adsorption

During the doping process there are two possible error sources: first the opening time of the shutter and, second, the uncontrolled adsorption of residual gas atoms during the doping process. In order to minimize both we decided to fix the evaporation time to roughly 1 minute. This was achieved via a separate calibration processes for each doping level. The exact doping level is defined via the time between the opening and the closing of the shutter. As it turns out, this error was always below 5%, for some measurements even below 1%.

The doping concentration was controlled via the opening time of the shutter and by the Ag flux via the evaporation temperature at the source. This temperature was adjusted so that the duration of the doping process was always between 30 and 60 s. These adjustments made it necessary to make a separate time calibration of the evaporator for each doping level with the positive side effect, that it was possible to get an idea of the error of the doping process.

As already mentioned in [28], doping by Ag competes with doping by residual gas in our case, but doping Ag atoms already present on the surface passivate it, so that it is most sensitive to residual gas only at the lowest doses of excess Ag. Since our EELS scans typically take between 20 and 30 min per spectrum, this issue cannot be neglected here. The time necessary for cooling and for doping has to be added, but measuring times were always dominant. This time, starting right after high temperature annealing of the surface, was recorded. In order to separate any kind of residual gas effects from those to be actually measured, and in order to be able to compute a viable error bar, we made time dependent EELS measurements for each doping step in order to post-process the data using an exponential adsorption model for filling the doping sites. Using the time stamps of the

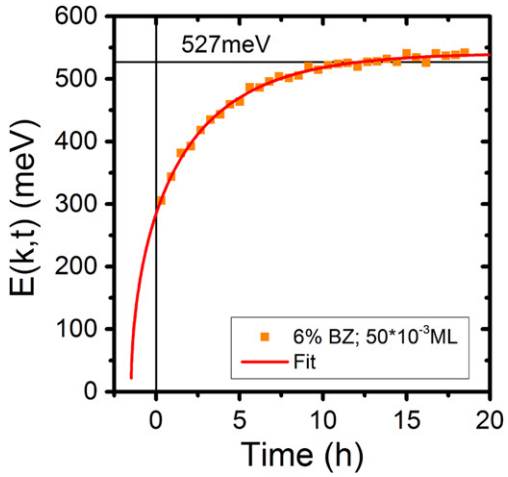

Figure 8. Time evolution of the position of the plasmon loss peak after adsorption of 0.05 ML of Ag on Si(557) at $k_{\|} = 6\%$ BZ. The solid line is a fit assuming a fixed number of doping adsorption sites, only direct adsorption with a constant sticking coefficient. This results in an exponential approach to saturation. The extrapolation to time zero was used to identify the effect of pure Ag doping.

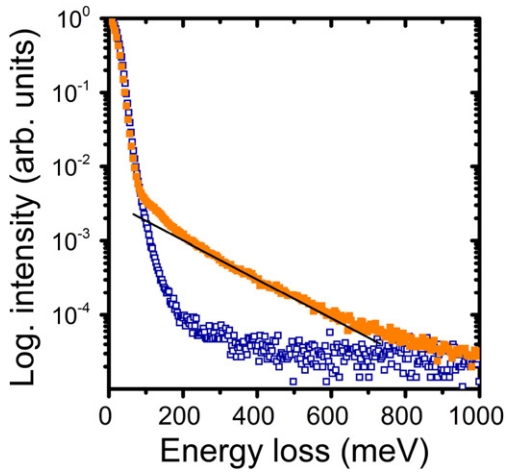

Figure 9. Inelastic background of Ag on Si(557) at $k_{\|} = 0$ for an undoped semi-metallic layer at a coverage of 1ML (open symbols) compared with that after adsorption of 1.2 ML of Ag at 500 °C. Incident electron energy 20 eV.

measurement and the starting point of the doping process we are able to extrapolate to an adsorbate-free surface. An example is shown in figure 8 for an Ag coverage of 0.05 ML.

Appendix B. Data evaluation of EELS spectra

Here we explicitly explain our method of fitting EELS spectra. It is rationalized by the experimental finding in many examples of low-dimensional metallic systems, that there is always a significant increase in structureless background once the layer becomes metallic. In the example shown in figure 9, we compare Ag on Si(557) with coverages close to 1 ML. For the lower data set doping was completely removed, while for the other one doping is close to saturation. This background outside the quasi-elastic peak is dominated by an exponential decay, generally called Drude tail, which varies as a function of electron energy and of detection angle $(k_{\|})$, but its general form always remains. It is the result mostly of multiple inelastic electron scattering within the metallic layer [40], but no analytic expression exists for it. Therefore, our approach has to be viewed as a parametrization, which, however, can be rationalized as follows: also the low-dimensional metal possesses a continuum of single and multiple intra- and interband excitations with short life times, which, due to the large interaction of excited electrons are also multiply scattered.

Since an exact analysis of all the possible combinations of excitations and the corresponding probability could only be done via the extensive use of Feynman diagrams, we choose a much simpler way: assuming as a

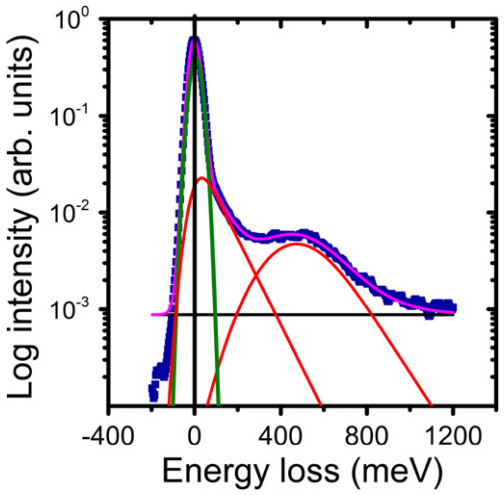

Figure 10. Example of the fit of a typical EELS spectrum with the functions described above. Note the semi-log scale. Shown are elastic peak (green), fits of Drude tail and loss peak by EMG-functions (red, see also text), and their sum (magenta) in comparison with the measured loss spectrum (blue symbols). The example is for saturation doping at $k_{\|} = 0.13\text{Å}^{-1}$.

first approximation the form of the Drude tail to be dominated by combinations of the energetically smallest possible intraband excitations (e.g. a non-zero energy signature can be achieved via an interband excitation as well as by a diverging number of infinitesimally small intraband excitations), we limit ourselves to the case of intraband excitations of infinitesimal energies and a constant excitation probability below but close to one. In this simple picture it is clear that the probability for an arbitrary energy loss must depend exponentially on the number of intraband excitations needed. Summing over all possible loss energies, under the assumption that the energy signature is Gaussian-like, one can make the transition to an integral, if the probability of a single intraband excitation increases with decreasing excitation energy:

$$f(E) = \frac{A}{\tau\rho\sqrt{2}} \int_0^\infty \exp\left(-\frac{y}{\tau}\right) \cdot \exp\left[-\frac{\left(E - E_0 - y\right)^2}{2\rho^2}\right] \mathrm{d}y. \tag{7}$$

Note that E_0 can also be 0, which corresponds to the loss tail of the elastic peak. ρ characterizes the intrinsic width of the excitation at E_0, A the amplitude and τ corresponds to the excitation probability of the single intraband excitation. Using basic mathematics one can reduce the above form to:

$$f(E) = \frac{A}{2\tau} \exp\left[\frac{E_0 - E}{\tau} - \frac{\rho^2}{2\tau^2}\right]\left(1 - \mathrm{erf}\left[\frac{E_0 - E}{\sqrt{2}\rho} - \frac{\rho}{\sqrt{2}\tau}\right]\right). \tag{8}$$

This exponentially modified Gaussian form (EMG) with the parameters A, ρ and τ was used in our fits in order to extract peak positions and halfwidths. An example is shown in figure 10.

References

[1] Stern F 1967 *Phys. Rev. Lett.* **18** 546
[2] Pitarke J M, Silkin V M, Chulkov E and Echenique P 2007 *Rep. Prog. Phys.* **70** 1
[3] Silkin V M, Garcia-Lekue A, Pitarke J M, Chulkov E V, Zaremba E and Echenique P M 2004 *Europhys. Lett.* **66** 260
[4] Nagao T, Yaginuma S, Inaoka T and Sakurai T 2006 *Phys. Rev. Lett.* **97** 116802
[5] Chen J *et al* 2012 *Nature* **487** 77
[6] Fei Z *et al* 2012 *Nature* **487** 82
[7] Law S, Yu L, Rosenberg A and Wasserman D 2013 *Nano Lett.* **13** 4569
[8] Ibach H and Mills D L 1982 *Energy Electron Loss Spectroscopy and Surface Vibrations* (San Francisco: Academic)
[9] Bill A, Morawitz H and Kresin V Z 2003 *Phys. Rev.* B **68** 144519
[10] Diaconescu B *et al* 2007 *Nature* **448** 57
[11] Park S and Palmer R 2010 *Phys. Rev. Lett.* **105** 016801
[12] Pohl K, Diaconescu B, Vercelli G, Vattuone L, Silkin V M, Chulkov E V, Echenique P M and Rocca M 2010 *Europhys. Lett.* **90** 57006
[13] Jahn M, Muller M, Endlich M, Neel N, Kröger J, Chis V and Hellsing B 2012 *Phys. Rev.* B **86** 085453
[14] Vattuone L, Smerieri M, Langer T, Tegenkamp C, Pfnür H, Silkin V, Chulkov E V, Echenique P M and Rocca M 2013 *Phys. Rev. Lett.* **110** 127405
[15] Smerieri M, Vattuone L, Savio L, Langer T, Tegenkamp C, Pfnür H, Silkin V M and Rocca M 2014 *Phys. Rev. Lett.* **113** 186804
[16] Langer T, Förster D, Busse C, Michely T, Pfnür H and Tegenkamp C 2011 *New J. Phys.* **13** 053006
[17] Politano A, Marino A R, Formoso V, Farias D, Miranda R and Chiarello G 2011 *Phys. Rev.* B **84** 033401

[18] das Sarma S and Hwang E H 1996 *Phys. Rev.* B **54** 1936–46
[19] Nagao T, Yaginuma S, Inaoka T, Sakurai T and Jeon D 2007 *J. Phys. Soc. Japan* **76** 114714
[20] Liu C, Inaoka T, Yaginuma S, Nakayama T, Aono M and Nagao T 2008 *Phys. Rev.* B **77** 205415
[21] Block T, Baringhaus J, Tegenkamp C, Inaoka T and Pfnür H 2011 *Phys. Rev.* B **84** 205402
[22] Rugeramigabo E P, Tegenkamp C, Pfnür H, Inaoka T and Nagao T 2010 *Phys. Rev.* B **81** 165407
[23] Allen S J, Tsui D C and Logan R A 1977 *Phys. Rev. Lett.* **38** 980–3
[24] Jusserand B, Richards D, Fasol G, Weimann G and Schlapp W 1990 *Surf. Sci.* **229** 394
[25] Hasegawa S, Tong X, Jiang C S, Nakajima Y and Nagao T 1997 *Surf. Sci.* **386** 322–7
[26] Liu Y and Willis R F 2009 *Surf. Sci.* **603** 2115–9
[27] Krieg U, Brand C, Tegenkamp C and Pfnür H 2013 *J. Phys.: Condens. Matter* **25** 014013
[28] Krieg U, Zhang Y, Tegenkamp C and Pfnür H 2014 *New J. Phys.* **16** 043007
[29] Nagao T, Hildebrandt T, Henzler M and Hasegawa S 2001 *Phys. Rev. Lett.* **86** 5747
[30] Crain J N, Gallagher M C, McChesney J L, Bissen M and Himpsel F J 2005 *Phys. Rev.* B **72** 045312
[31] Nagao T and Hasegawa S 2000 *Surf. Interface Anal.* **30** 488–92
[32] Claus H, Büssenschütt A and Henzler M 1992 *Rev. Sci. Instrum.* **63** 2195
[33] Nakajima Y, Takeda S, Nagao T, Hasegawa S and Tong X 1997 *Phys. Rev.* B **56** 6782–7
[34] Nakajima Y, Uchida G, Nagao T and Hasegawa S 1996 *Phys. Rev.* B **54** 14134–8
[35] Sato N, Nagao T and Hasegawa S 1999 *Phys. Rev.* B **60** 16083–7
[36] Ueno M, Matsuda I, Liu C and Hasegawa S 2003 *Japan. J. Appl. Phys.* **42** 4894–7
[37] Oh D H, Kim M K, Nam J H, Song I, Park C Y, Woo S H, Hwang H N, Hwang C C and Ahn J R 2008 *Phys. Rev.* B **77** 155430
[38] Teys S A, Romanyuk K, Zhachuk R and Olshanetsky B 2006 *Surf. Sci.* **600** 4878–82
[39] Inaoka T 2014 private communication
[40] Persson B N J and Demuth J E 1984 *Phys. Rev.* B **30** 5968–86